



## Digital Data Acquisition System for experiments with segmented detectors at National Superconducting Cyclotron Laboratory

K. Starosta<sup>a,\*</sup>, C. Vaman<sup>a</sup>, D. Miller<sup>a</sup>, P. Voss<sup>a</sup>, D. Bazin<sup>a</sup>, T. Glasmacher<sup>a</sup>, H. Crawford<sup>b</sup>, P. Mantica<sup>b</sup>, H. Tan<sup>c</sup>, W. Hennig<sup>c</sup>, M. Walby<sup>c</sup>, A. Fallu-Labruyere<sup>c</sup>, J. Harris<sup>c</sup>, D. Breus<sup>c</sup>, P. Grudberg<sup>c</sup>, W.K. Warburton<sup>c</sup>

<sup>a</sup> National Superconducting Cyclotron Laboratory and Department of Physics and Astronomy, Michigan State University, East Lansing, MI 48824, USA

<sup>b</sup> National Superconducting Cyclotron Laboratory and Department of Chemistry, Michigan State University, East Lansing, MI 48824, USA

<sup>c</sup> XIA LLC, Hayward, CA 94544, USA

### ARTICLE INFO

#### Article history:

Received 24 June 2009

Received in revised form

2 September 2009

Accepted 4 September 2009

Available online 15 September 2009

#### Keywords:

Digital data acquisition

Segmented Ge detector array

$\gamma$ -Ray tracking

### ABSTRACT

A 624-channel Digital Data Acquisition System capable of instrumenting the Segmented Germanium Array at National Superconducting Cyclotron Laboratory has been implemented using Pixie-16 Digital Gamma Finder modules by XIA LLC. The system opens an opportunity for determination of the first interaction position of a  $\gamma$  ray in a SeGA detector from implementation of  $\gamma$ -ray tracking. This will translate into a significantly improved determination of angle of emission, and in consequence much better Doppler corrections for experiments with fast beams. For stopped-beam experiments the system provides means for zero dead time measurements of rare decays, which occur on time scales of microseconds.

© 2009 Elsevier B.V. All rights reserved.

### 1. Introduction

A 624-channel Digital Data Acquisition System (DDAS) for pulse shape analysis of signals from segmented radiation detectors has been implemented recently at National Superconducting Cyclotron Laboratory (NSCL). The system is primarily designed to operate in conjunction with the Segmented Germanium Array (SeGA) [1] for in-beam studies which combine identification of reaction residues (see for example Ref. [2]) with  $\gamma$ -ray detection. DDAS has been successfully used in a number of in-beam experiments at NSCL providing data which open an opportunity for identification of positions of interactions for  $\gamma$  rays within SeGA detector crystals by pulse shape analysis of digitized signals. The subsequent  $\gamma$ -ray tracking [3], when combined with the tracking of heavy ions in a high resolution spectrograph such as the S800 [2], offers an opportunity to significantly improve  $\gamma$ -ray energy resolution in these measurements through more accurate Doppler corrections. Another main application of DDAS is for stopped-beam experiments investigating charged-particle decay of ions following implantation. In these studies, DDAS provides means for zero dead time measurements of rare decays, which occur on time scales of microseconds. The

current status of DDAS, its applications, and first experimental results are discussed.

### 2. A SeGA detector

While Ref. [1] discusses the  $\gamma$ -ray detectors of SeGA in detail, it is worthwhile to reiterate here information which is most relevant to the implementation of DDAS. The outer contact of a n-type coaxial HPGe SeGA detector is divided into eight slices longitudinally and into four quarters azimuthally which results in the 32-fold segmentation shown in Fig. 1. Each of the segments and the central electrode of a detector are served by a room temperature Field Effect Transistor (FET) and a charge-sensitive preamplifier designed to have 30/40 ns risetime at 0/45 pF, 50  $\mu$ s decay time constant, and gain of 120 mV/MeV. A single SeGA detector thus requires 33 channels of electronics to be fully instrumented. A full array may consist of up to 18 detectors.

### 3. Requirements for DDAS

The following capabilities are required for an acquisition system to provide data for  $\gamma$ -ray tracking from SeGA in a typical NSCL experiment:

- Capability to instrument all 594 SeGA channels and possibly auxiliary detectors.

\* Corresponding author. Current address: Department of Chemistry, Simon Fraser University, 8888 University Drive, Burnaby, BC, Canada V5A 1S6. Tel.: +1778 782 8861; fax: +1778 782 3765.

E-mail address: [starosta@sfu.ca](mailto:starosta@sfu.ca) (K. Starosta).

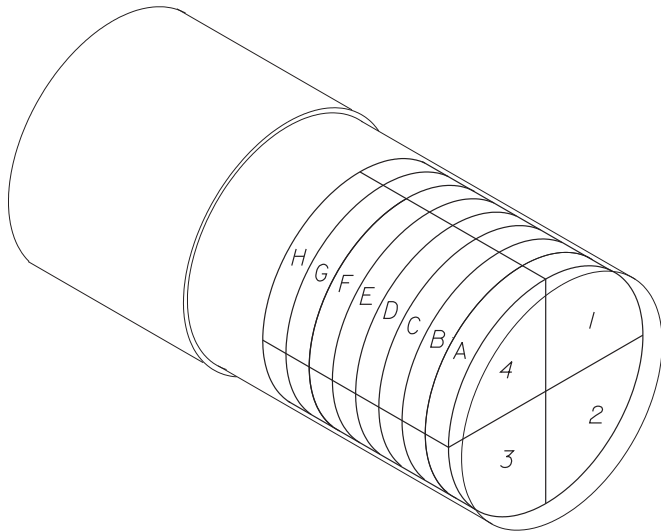


**Fig. 1.** Segmentation and naming convention used to label quarters and slices of Segmented Germanium Array detectors. In a typical experimental setup, quarters 2 and 3 face the beam.

- In response to a common trigger, a capability to capture waveform information with a 100 MHz sampling rate for selected channels synchronously with a jitter of  $< 1$  ns.
- Capability to capture  $1 \mu\text{s}$  long waveforms with rise time information for detectors in which interactions occurred at a trigger rate of at least 1000 counts per second for the full SeGA array.
- Capability to measure pulse height and accumulate Multi-channel Analyzer (MCA) histograms in real time at the rate of 10,000 counts per second for a single SeGA detector without deterioration of energy resolution as compared to a state-of-the-art analog system.
- Capability to operate with near zero dead time.
- Capability to integrate with other data acquisition systems.
- Capability to provide data for analysis in near or real time.

DDAS was designed to provide the above capabilities and a series of tests were conducted to verify the performance of the system.

#### 4. Implementation and architecture of DDAS

DDAS has been implemented using Pixie-16 Digital Gamma Finder (DGF) modules by XIA LLC taking advantage of their high on-board computing power, flexibility, and fast protocols for module-to-module communication, as well as their high-performance, on-board, and real-time pulse-shape analysis algorithms for extracting energy information from Ge  $\gamma$ -ray detectors. A single Pixie-16 card provides means for analysis of 16 signals via a 12-bit 100 MHz Flash Analog to Digital Converter (FADC) allocated for each channel. The number of channels per card naturally drives a separation of the central core and  $2 \times 16$  segment signals for a single detector in the DDAS architecture. This separation, in turn, drives the requirements for clock and trigger distribution in the system. Custom firmware has been developed by XIA LLC in collaboration with NSCL to handle the DDAS application using Pixie-16 modules. Detailed information on the technical implementation, including trigger and clock distribution, has been reported in Refs. [4,5]; the information most relevant for application in NSCL experiments is summarized below.

DDAS is comprised of 39 Pixie-16 modules organized into four custom-made CompactPCI/PXI crates as shown in Fig. 2. Special



**Fig. 2.** DDAS (left) with its computer cluster (right). Note the Central Unit (see text for details) which is the second crate from the top as indicated by the ribbon cables connecting the Director to the VME crate holding a CAEN 1495 FPGA module used for trigger integration with acquisition systems other than DDAS.

care has been taken to assure that the clock distributed between the crates of DDAS results in synchronous capture of the waveforms within the specified jitter limit [5]. Custom DDAS modules were developed by XIA LLC for inter-crate clock distribution, while the distribution between modules in a single crate proceeds via the backplane. The results of the clock tests are reported in Section 7.1.

Each CompactPCI/PXI crate is connected to a Linux PC server via a National Instruments MXI-4 PXI-PCI optical bridge. Four of the crate servers and a fifth event-building server are linked via a Gigabit network into a 10 TB Sun data storage system and constitute the DDAS Computer Cluster (see Fig. 2). The readout FIFO of each DDAS Pixie-16 module is polled and read out separately by the server associated with the respective crate. As a result, 39 files containing DDAS data are written simultaneously during data acquisition. The data transfer is limited by the CompactPCI/PXI crate backplane to  $\sim 100$  MB/s.

All Pixie-16 modules in DDAS have identical hardware. Moreover, the firmware loaded for DDAS operation is identical for each card. However, cards differ by the roles they play in the data acquisition. The role for a particular card in the system is selected via a set of jumpers and by configuration parameters loaded during the system initialization.

The roles of the cards are as follows. A single card called the Director is responsible for receiving and distributing triggers

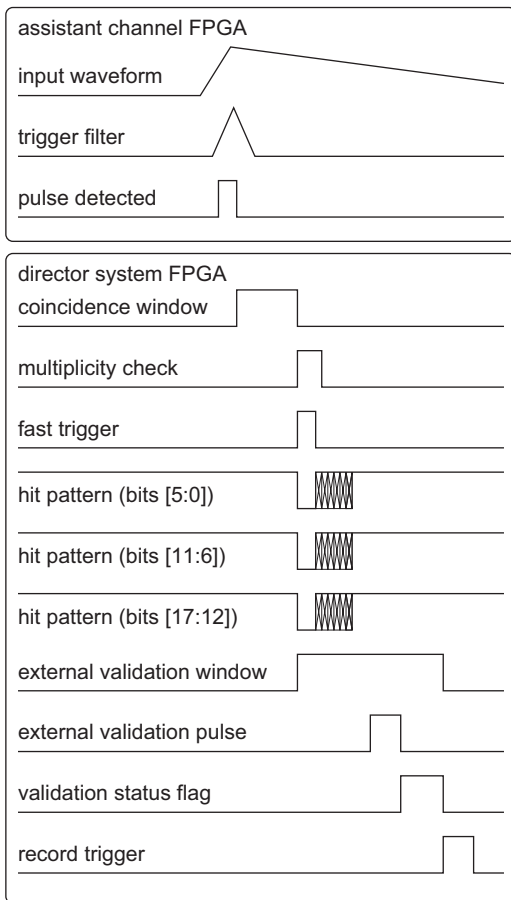


Fig. 3. Timing diagram for DDAS triggers, see text for details.

within the DDAS system as well as for communication and event integration with external data acquisition systems serving devices other than SeGA. Two cards called Assistants are responsible for capturing waveforms and energies from central cores of SeGA in channels 0–8, and auxiliary detectors in channels 9–15. The other 36 cards form Manager/Worker pairs capturing waveforms and energy information from segments of SeGA detectors with a single Manager/Worker pair instrumenting all 32 segments of a single SeGA detector. The Director and two Assistants are hosted in a single CompactPCI/PXI crate called Central Unit, with the Director located between the Assistants; the Manager/Worker pairs are distributed between the remaining three CompactPCI/PXI crates.

In the current firmware configuration, DDAS captures and stores waveform and energy information for the central contact and all segments of a detector if the energy deposited by a  $\gamma$ -ray interaction is above the threshold set for its central contact. This is motivated by the fact that tracking algorithms for SeGA have not yet been developed and it is unclear how to optimize the readout scheme by segment selection. It should be noted that a targeted readout of selected segment waveforms is possible with the DDAS hardware by a firmware modification and provides the potential for further improvement of DDAS speed and performance.

Fig. 3 shows the timing diagram for the current implementation of DDAS triggering based on the information from SeGA central cores. Field-Programmable Gate Arrays (FPGA's) which process SeGA signals on Assistant modules run fast trapezoidal filter algorithms which are configured to respond to  $\gamma$ -ray signals of interest. Logic pulses indicating detection of  $\gamma$  rays in SeGA central contacts are transmitted via a backplane of the Central Unit from Assistants to the Director. Assistant modules are

installed immediately to the left and right of the Director in order to optimize the transfer of triggers through the backplane. In response to the first  $\gamma$  ray communicated, the Director opens a coincidence window with a user-defined length. At the end of the coincidence window, the following actions are taken:

- The Director opens a validation window of user-defined length. A validation pulse has to be received by the Director within this window to consider the event valid.
- The validation window signal becomes available on one of the analog outputs of the Director and can be used for monitoring or as a DDAS-issued trigger to other data acquisition systems. The delay of this signal with respect to the first  $\gamma$  ray in the event is  $\sim 360$  ns plus the length of the coincidence window.
- The Director computes the multiplicity of SeGA triggers received within the coincidence window.

If  $\gamma$ -ray multiplicity of an event satisfies the condition preset by the user, the following happens:

- The Director sends a fast trigger which signals the start of synchronous waveform capturing to all DDAS modules. Captured waveforms have user-defined length and include a user-defined time interval before the fast trigger. Modules receiving the fast trigger latch a time stamp provided by the common 100 MHz DDAS clock, and increment and latch their event number counter.
- The fast trigger is followed by the hit pattern which identifies modules for which the waveform/energy information is to be stored for readout. Based on the decoded hit pattern a module recognizes if a  $\gamma$ -ray interaction occurred in the detector it serves. The fast trigger/hit pattern is distributed between modules via a serial trigger distribution link. Custom DDAS trigger modules have been built by XIA for that purpose. DDAS Pixie-16 modules indicated by the hit pattern store the waveform/energy information for potential readout.
- The fast trigger and SeGA hit pattern information are made available on a parallel Low Voltage Differential Signaling (LVDS) link for processing via external modules. In the current implementation of DDAS, this information is passed to the CAEN 1495 FPGA module with NIM input and output. The CAEN 1495 module then can be used to integrate DDAS triggering with other data acquisition systems. In particular, this module can be used to issue a validation pulse to DDAS.

If the validation pulse is detected within the validation window and the multiplicity of  $\gamma$ -ray events meets the user-preset threshold, the Director issues a Record Trigger to all DDAS modules at the end of the validation window. Modules indicated by the hit pattern, upon receiving the Record Trigger, respond by assembling a header, energy, and waveform information into an event stored in the module FIFO. Stored events are then read out from FIFOs in block mode by the server operating the respective crate. If the Record Trigger is not issued by the Director, events are overwritten on the next fast trigger.

Several optimizations implemented to execute the above triggering scheme to satisfy the DDAS requirements are worth mentioning.

- While the synchronous waveform capturing is triggered on the common fast trigger, the energy measurement has to be done with respect to the trigger local to the channel of interest to assure the best energy resolution. This adds to the complexity of the firmware, but has been verified to work properly, see Section 7.3.

- A sophisticated scheme of captured waveform storage and transfer within the card was developed to minimize DDAS dead time. In this so-called “Zero Dead Time” solution the waveforms are first stored in a memory buffer local to the processing channel. Depending on the waveform length the memory buffer on a single channel can store multiple waveforms (38 for 1  $\mu$ s waveforms), thus a subsequent waveform can be stored right after the processing of the previous one has ended. The waveforms are transferred to the module FIFO for readout. The transfer can occur when the module is storing newly captured waveforms to the memory buffer. This is because the memory buffer is dual ported, i.e. reading from and writing to the memory buffer can happen simultaneously. This also ensures that the dead time is eliminated when events are transferred from each channel’s memory buffer to the module FIFO. The “zero dead time” achieved for DDAS is documented in Section 7.2.
- A Manager/Worker pair can communicate to each other through their nearest neighboring lines on the backplane without interfering with the operation of any other modules. In the current implementation, this feature is used to synchronize filling and readout of the FIFOs for a pair such that a full segment data set for a detector is either delivered or dropped. However, an option is available through future firmware upgrades for the Manager/Worker pair to decide on waveform readout of segments which have actual deposited or induced charges. This selection can be achieved through Manager/Worker communication of readout lookup tables defined based on future-implemented tracking algorithms.
- SeGA waveform pulses can be delayed inside the Pixie-16 signal processing chain to accommodate coincidences with slow detectors. This delay can be adjusted up to 2.56  $\mu$ s to overlap the validation window, since a validation pulse may arrive with a considerable delay with respect to SeGA triggers. This delay is equivalent to cable delay; however, there is no signal deterioration, since the signals have already been digitized.

The results for the DDAS implementation discussed above are given in Section 7.

## 5. DDAS event building

The server allocated to each DDAS crate continuously checks the status of module FIFOs through the MXI-4 optical bridge and the backplane. If a FIFO is reported as ready for readout, the data is transferred in block mode to the storage array and written into a file associated with the module. Thus a full DDAS data stream consists of up to 39 files containing so-called “module events”. The operating outside DDAS opens and closes these files at the beginning and end of a run, respectively.

Pixie-16 modules continue to take data as events are being read from their FIFOs. In this respect, the communication between Manager and Worker is crucial for keeping the data stream synchronized for a single detector at high rates. Indeed, let us assume that the FIFO of both Manager and Worker are full and ready for readout. When one of them is read out and emptied it could start receiving data, while the other one is still full. Differences in FIFO contents created in this way, which could lead to significant data losses, are specifically prevented by the DDAS firmware.

There are two means by which data from module events are assembled into analysis-ready DDAS events—an event number and a DDAS 100 MHz time stamp, both saved in a module event header. Event-building software written at NSCL assembles DDAS

events based on the user-provided mapping of DDAS modules to physical detectors. Event building starts with the Director data containing the DDAS hit pattern, and proceeds through the Assistants data for SeGA detector central contacts, and Manager/Worker pairs data for SeGA detector segments. DDAS events assembled based on the event number are required to share a common time stamp. The event-building software is robust enough to handle information loss from missing Assistant or Manager/Worker data, which happen at high trigger rates.

In the current implementation, the event building is based on the data written to the storage array. This is mainly a factor of the computing complexity since the current solution involves six workstations and two networks of different speed which results in variable delay times for real-time access to the data. Event building from stored data implies that a run has to be completed before it can be examined. This results in a delay of data monitoring on the level of the full DDAS or a complete SeGA array. The event-building software is fast enough to provide the data for analysis in near real time, shortly (less than a minute for a typical in-beam experiment) after the end of the run. However, to aid real-time data monitoring a number of programs have been developed to examine the module events as statistics are collected. These programs access the files opened for event recording, and include a waveform display and an energy histogram sorter. Also, energy histograms are collected by the firmware of Pixie-16 modules and can be written to disk on user request. As a result, DDAS is robust, reasonably easy to set-up and handle, and has established a record of reliable performance in a number of in-beam and radioactive-decay experiments. Real-time data analysis and monitoring are under development.

## 6. Integration with other detectors at NSCL

Integration of SeGA and DDAS with other devices and data acquisition systems is one of the crucial experimental requirements at NSCL. So far, SeGA with DDAS has been integrated with the S800 [2], the Sweeper Magnet spectrograph, a phoswich detector for heavy-ion identification, and a double sided silicon strip detector for  $\alpha$ - $\gamma$  angular correlation measurements. In all cases the DDAS and charged-particle data streams were stamped with a 1 MHz clock, stored separately, and merged in near real time for analysis.

The time stamping of DDAS and spectrograph data streams is implemented as follows. A 48-bit counter is set up on the Director module of DDAS. This counter is incremented whenever a TTL signal is provided on a specified analog input of the Director module. A corresponding 48-bit counter was organized for each analog data acquisition system of interest; in particular for the spectrographs it was implemented on an XLM FPGA module. The clock signals are then sent from a 1 MHz common pulser to both DDAS director and the analog counter, the counters are latched by the trigger (for DDAS by the validation pulse), and saved in a header of the stored event (for DDAS in the Director header). After a run is completed, the data streams are merged based on the common time stamp.

Again, analysis programs have been developed at NSCL to handle merging and monitoring of the data streams. Merging is done in three steps. First, DDAS events are built as described in Section 5. DDAS events are then reduced into a data stream equivalent to that of an analog SeGA data stream by partial signal analysis and omission of the waveforms. Finally, the reduced data stream is merged with the analog data stream. One of the five DDAS cluster computers is dedicated to data merging only.

The second step of the merging process allows the near real-time analysis of NSCL on-line data using programs developed for

monitoring SeGA with an analog data acquisition system. Currently, the waveform analysis done at merging is limited to the constant fraction timing between SeGA and E1 scintillator in the S800 focal plane as described in Section 7.4. For a typical in-beam run, a merged data file is available within a minute after the run is ended. It should be stressed that both the DDAS and spectrograph's raw data streams are saved and can be monitored separately and that re-merging or more advanced analysis can be done off-line.

## 7. Performance and results

### 7.1. Clock distribution

The information on a position of  $\gamma$ -ray interaction within a segmented Ge detector is encoded in rise times of the induced and real signals. Therefore, the synchronous waveform capturing is one of the necessary and crucial conditions for implementation of  $\gamma$ -ray tracking for SeGA. When evaluating the capability of a data acquisition system to capture synchronous waveforms within a set of distributed modules one has to distinguish between a true jitter of the clocks and a relative shift of a time reference, which may be related to cable delays or delays in analog pre-processing. While the latter can be calibrated and compensated for, the former cannot and defines the true limitation of the system.

Relative delays and jitters between DDAS modules serving SeGA central contacts and corresponding segments were measured using a precise sine wave generator. First, the sine wave generator was set to 0.5 MHz and 35  $\mu$ s-long waveforms were collected. The frequency of the sine wave measured by DDAS was extracted and histogrammed for a large set of events. The agreement between the generator and DDAS fits, which included the fundamental and the second harmonic, was better than 2 Hz. Next, the sine waveform from the generator was split two-fold and sent by cables of equal length into a reference channel on an Assistant and a channel of interest on a Manager/Worker pair; 2  $\mu$ s waveforms were collected for both channels. For both waveforms a phase shift relative to the DDAS 100 MHz clock was extracted on an event-by-event basis using a  $\chi^2$  fit assuming the 0.5 MHz frequency of the fundamental sine wave and a

presence of the second harmonic. The difference between these phase shifts was histogrammed and analyzed. For a given DDAS channel, the centroid of the histogram represents the time shift relative to the reference while the standard deviation represents the clock's jitter. A histogram of time shifts and jitters for 15 SeGA detectors set up for the 2009 DDAS SeGA campaign is shown in Fig. 4. As seen from the right panel of Fig. 4 the 1 ns jitter requirement is easily met by the system, and one can conclude that waveforms are collected by DDAS synchronously.

### 7.2. Dead time

The performance of the “Zero Dead Time” solution was tested using DDAS working in a stand-alone mode, meaning, without interfacing with other data acquisition systems, which could potentially impose their dead time on the measurement. A series of data sets were collected at varying count rates on SeGA detectors and the time distribution between consecutive events was then examined from the data. An example of the analysis is shown in Fig. 5. The results of the measurements clearly indicated that up to the upper limit of 1000 counts per second, specified in the requirements for DDAS, event losses were consistent with that expected for pile-up rejection defined by the settings of the slow filter for energy measurement. It was concluded, therefore, that the primary DDAS dead time is that of the energy measurement algorithm, while hardware/firmware dead times are negligible from the point of view of envisioned applications.

### 7.3. Energy resolution

A real-time algorithm used for energy measurement from digitized waveforms in DDAS has been implemented in the Pixie-16 card firmware delivered by XIA. The Pixie-16 cards' good performance for  $\gamma$ -ray energy measurement was one of the motivating factors for selecting this particular hardware solution for the implementation of DDAS. The energy measurement algorithm has been verified with standard Ge detectors as described in Ref. [4]. One should note that for a SeGA detector, the energy resolution is limited by the noise level of warm FETs [1] used to extract signals from the central core and the segments.

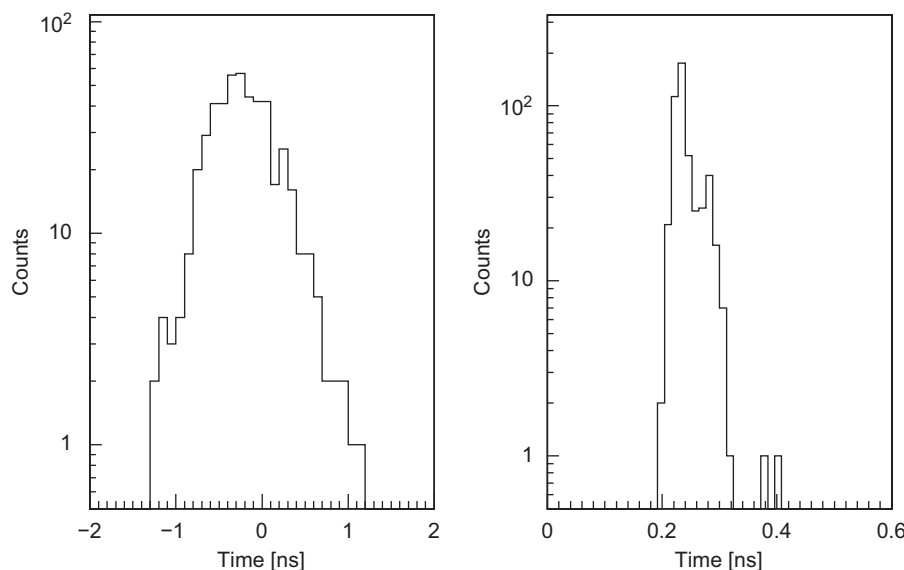
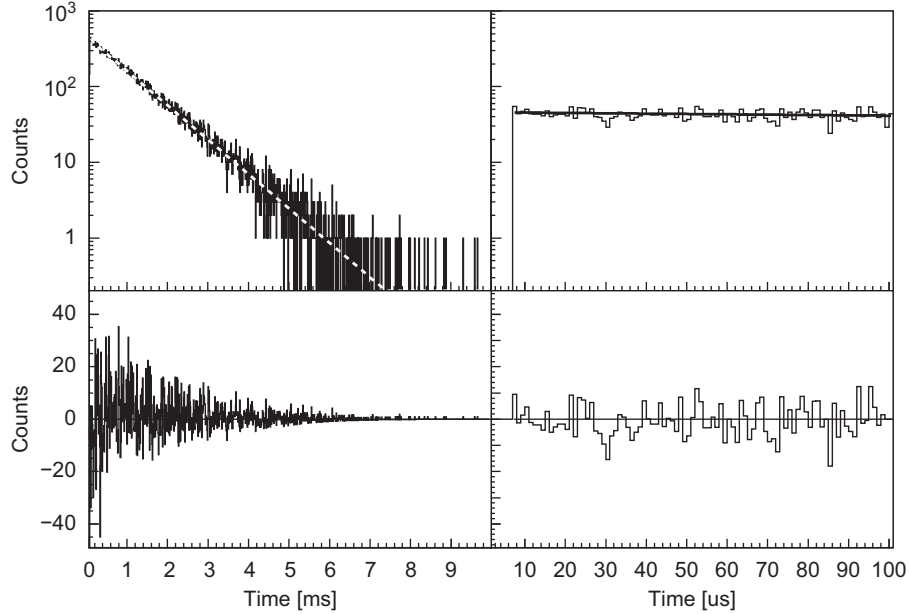


Fig. 4. A histogram of clock time shifts (left) and clock time jitters (right) for the 2009 DDAS SeGA campaign, see text for details.



**Fig. 5.** Time distribution between neighboring events detected by DDAS in a stand alone mode. Left panels present the data for time differences up to 10 ms with a binning of 10  $\mu$ s per channel; right panels present the same data up to 100  $\mu$ s with a binning of 1  $\mu$ s per channel. The top panels show the time differences between neighboring events with a fit of a single exponential function superimposed. The fit yields an expected average count rate of  $990 \pm 5$  counts per second which is used consistently for the plots independent of a histogram binning. The reduced  $\chi^2$  for the fit is 0.7. The bottom panels show residual differences between the data and the fit. A good agreement with the exponential distribution expected for time differences, as shown by left panels, indicates practically negligible data losses within DDAS. The loss of events separated by less than  $\sim 7 \mu$ s, visible in right panels, is a consequence of the pile-up rejection; in this measurement the window for energy-filter pile-up inspection was set to 6  $\mu$ s.

As a result, the energy resolution measured by DDAS for SeGA central cores has always matched the energy resolution measured with a corresponding analog setup.

Several procedures were developed to facilitate the calibration of large number of SeGA channels involved in DDAS experiments. While the energy calibration of the central contacts is standard, the calibration of the segments needs to account for capacitive coupling and cross-talk which in turn depends on the location of the segments in which the  $\gamma$ -ray interaction occurred, see for example Ref. [6]. Proper cross-talk correction for SeGA detectors is under investigation based on the data collected with DDAS; the results will be published in a forthcoming paper. A phenomenological  $\chi^2$  fit described below has currently been implemented, and yields a satisfactory segment energy resolution.

For the discussion below, let the segment fold be defined as the number of segments in which net charge has been deposited. Calibration coefficients for segments in a SeGA detector without the cross-talk correction become fold-dependent, which in principle, implies that different sets of parameters are required for each segment fold. This is prohibitive, since the number of parameters needed for a given fold grows like the number of corresponding combinations, and, in addition to the practical difficulty in handling such a large parameter set, the statistics seldom can be accumulated to calibrate segments in the original fold of the event. The procedure described below overcomes this difficulty.

In the analysis, a second-order polynomial fit is employed to calibrate central contacts using data from standard sources. Knowing the central contact calibration parameters, a subset of the data with the  $\gamma$ -ray interaction confined within a single segment is used to extract segment fold-1 calibration parameters. For each detector, a  $\chi^2$  minimization is used to extract 32 sets of fold-1 segment parameters up to the second order by requiring the segment energy to be equal to the central core energy. An advantage of this minimization algorithm is that it does not require identification of  $\gamma$ -ray peaks and can be executed on any

data set (including room background) as long as the calibration of the central contact energy is reliable. An analogous  $\chi^2$  minimization is then employed to calibrate segment fold-2 events with the second order calibration parameters extracted for  $32 \times 31/2 = 496$  pairs of segments for each detector. The running time for the computer codes extracting fold-1 and fold-2 segment parameters is negligible compared to the time needed for manual calibrations of central contacts.

If carried out according to the above procedure, the number of parameters for segment fold-3 calibration is 10 times larger than for the segment fold-2 calibration. To overcome related inconveniences, calibration of segments for events with segment fold-3 and higher was done using the calibration coefficients extracted for folds-1 and -2 according to Eq. (1),

$$E^f = \sum_{k=1}^f E_k^1 + \sum_{k=1}^f \sum_{l=k+1}^f A_{k,l} + \frac{(f-1) * (f-2)}{2} * \delta \quad (1)$$

$$\Delta_{k,l} = E_{k,l}^2 - E_k^1 - E_l^1 \quad (2)$$

with  $E^f$  denoting a calibrated energy for segments with fold  $f > 2$ ,  $E_k^1$  denoting the energy for segment  $k$  calibrated with the corresponding calibration coefficients for fold 1,  $E_{k,l}^2$  denoting the energy for a pair of segment  $k, l$  calibrated with the corresponding calibration coefficients for fold 2. The  $\delta$  parameter denotes the nearly energy-independent  $\sim 4$  keV correction needed to align peaks in spectra observed at high folds. It most likely accounts for the capacitive coupling between the segments and the central core. It should be noted that for fold-1 and fold-2 the coupling between segments and the core is absorbed into the fitted coefficients. The detailed interpretation of the parameters in this procedure is being addressed by the ongoing investigation of the cross-talk parameters of SeGA detectors.

Energy calibrated spectra for one of the SeGA detectors is shown in Fig. 6. Calibrated segment spectra, when summed over the segment fold, have a resolution worse by a factor of  $\sim 2$  as

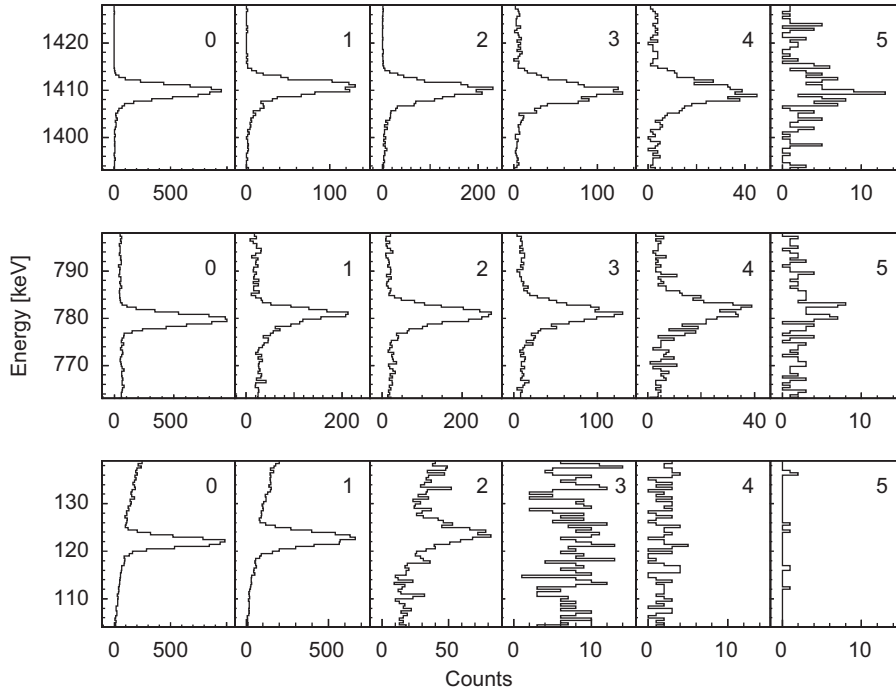


**Fig. 6.** Energy resolution as measured from the central contact (panels 0) and segment (panels 1–5) electrodes. For the segment spectra the label on the panel indicates the segment fold used in the calibration procedure given by Eq. (1). Bottom, middle, and top rows are for 121-, 778-, and 1408-keV transitions from a  $^{152}\text{Eu}$  source, respectively.

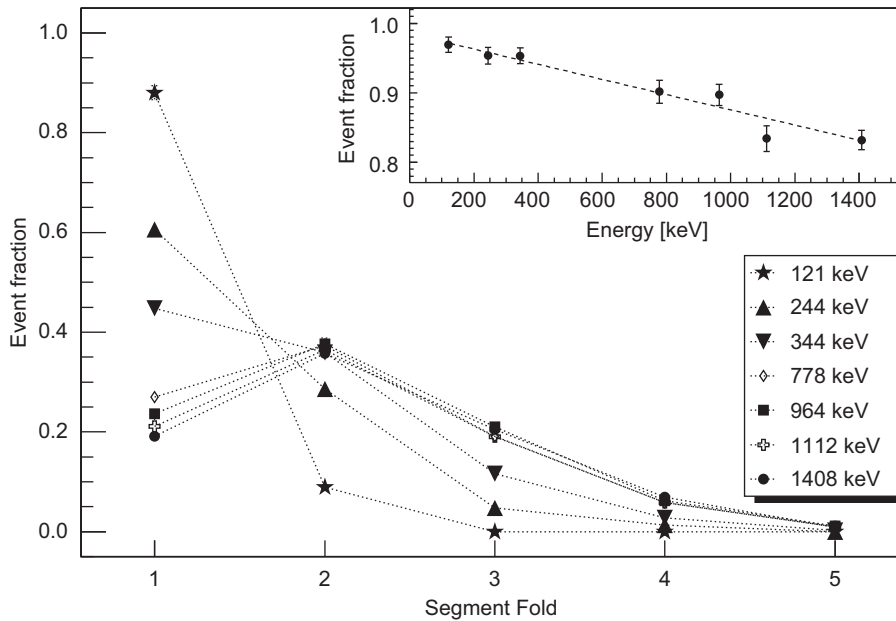


**Fig. 7.** (Main panel) Segment fold distribution as a function of  $\gamma$ -ray energy from spectra illustrated in Fig. 6. The event fraction on the ordinate is the intensity of a full energy peak measured in the segment spectrum at a given fold normalized to the intensity of the corresponding peak measured by the central contact. (Insert) Efficiency of full energy peak detection in segment spectra as a function of incident  $\gamma$ -ray energy. The event fraction on the ordinate is the intensity of a full energy peak measured in the segment spectra summed over all segment folds normalized to the intensity of the corresponding peak measured by the central contact.

compared to the spectrum for the central contact. Based on the spectra shown in Fig. 6 segment fold distribution has been measured as a function of detected  $\gamma$ -ray energy. The results presented in Fig. 7 show an expected shift of the segment fold distribution towards a higher mean value as the  $\gamma$ -ray energy increases from 121- to 778-keV. However, at higher energies, in particular the 778- to 1408-keV range explored from  $^{152}\text{Eu}$  calibrations, the changes of segment fold distribution are observed to be rather small.

Also, the insert in Fig. 7 shows the fraction of events detected in full energy peak when measured by the segments as compared to that measured by the central contact. The efficiency of full energy reconstruction in the standard calibration analysis described above varies between  $\sim 95\%$  at  $\sim 100$  keV to  $\sim 85\%$  at  $\sim 1.4$  MeV. The fact that the peak intensity as measured by segments is smaller than the corresponding intensity as measured by the central contact indicates the level of errors the algorithm is making in the segment fold determination. In the analysis, the

segment fold is incremented whenever an energy deposited within a segment is larger than a predefined threshold value. The setting of the threshold has a direct impact on the efficiency of the algorithm. The threshold set too high results in underestimated segment fold due to the loss of low energy deposits. The threshold set too low overestimates the fold, due to counting of induced signals or signals resulting from the cross-talk within the detector. Wrong fold determination results in incorrect energy calibration and, in consequence, in a good count appearing in a background rather than in a peak. Experience gained with the above analysis suggests that optimization of the threshold is not sufficient to bring the algorithm presented above to 100% efficiency. Therefore, an improved algorithm for segment energy calibration which takes into account the cross-talk corrections for measured signals is currently under development for SeGA detectors based on the data provided by DDAS.

#### 7.4. $\gamma$ -Ray timing

An extensive set of signals was measured using 1173- and 1332-keV coincident  $\gamma$  rays from a  $^{60}\text{Co}$  source as a step towards the envisioned implementation of a  $\gamma$ -ray tracking algorithm. The experimental setup included a fast CsF scintillator working in coincidence with the SeGA array and DDAS. The fast signals from the CsF detector with  $\sim 4\text{ ns}$  decay time cannot be digitized directly by the DDAS working with 10 ns sampling time. The analog signal from the CsF, therefore, was used to trigger a precision pulser which generated a  $50\ \mu\text{s}$  decay-time,  $\gamma$ -ray like pulse of fixed amplitude, which was subsequently input to one of the DDAS channels. The excellent timing properties of CsF combined with the fixed shape and delay of the pulser signal provided a very good time reference for comparison of waveforms recorded in subsequent events.

An algorithm extracting timing relationship between SeGA and CsF detectors has been implemented and tested using the data set described above. The algorithm takes advantage of the partial results from the trapezoidal energy filter analysis, which are provided on an event-by-event basis for each channel in the DDAS data stream. In particular, the baseline level and the amplitude for a waveform can be inferred from filter sums. The timing algorithm measures  $t_{10}$  and  $t_{20}$  parameters which correspond to the time at which a waveform reaches 10% and 20% of its amplitude, respectively. The time  $t_0$  is defined as the time corresponding to the intersection of the baseline with a line defined by the  $t_{10}$  and  $t_{20}$  values. The difference between  $t_0$  for a central contact and the reference CsF signal is plotted in Fig. 8. The lack of correlation between energy and time shown in the 2D spectrum in the bottom left panel of Fig. 8 indicates that the implemented algorithm sufficiently fulfills the role of a digital constant fraction discriminator; no energy dependent corrections were employed in the analysis. The root mean square resolution of the energy-integrated time peak is 16 ns, while the corresponding resolution for the 1332-keV  $\gamma$  ray is 10 ns.

Subsequently, this timing algorithm was incorporated into in-beam DDAS experiments. For the in-beam applications, the reference signal is provided by the precision pulser triggered by a plastic scintillator in the S800 object box [2]. The achieved time resolution is comparable to that from the source test, and certainly sufficient for applications of SeGA with DDAS in in-beam experiments at NSCL.

#### 7.5. Induced signals

The  $^{60}\text{Co}$  data set was examined to investigate amplitudes and shapes of signals induced by a  $\gamma$ -ray interaction within a SeGA

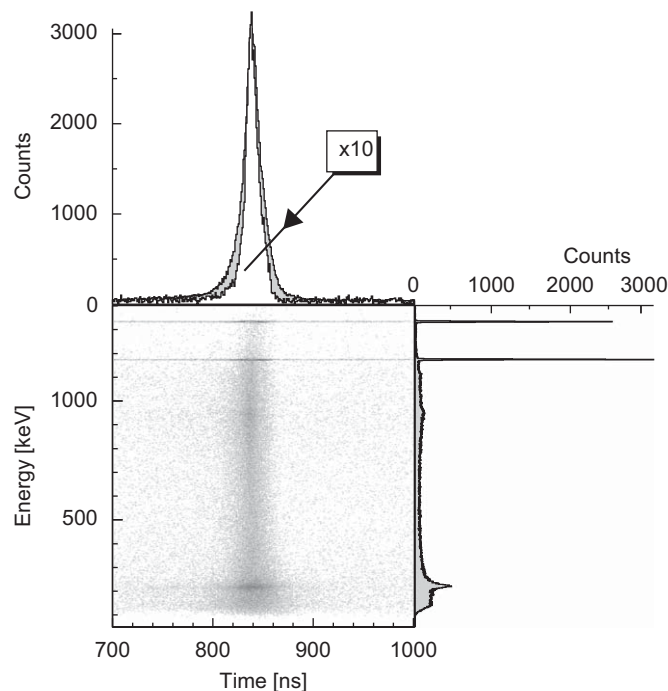


**Fig. 8.** Energy-time correlation matrix from a  $^{60}\text{Co}$  SeGA–CsF coincidence measurement (bottom left) including projections on the energy (bottom right) and time (top left) axes. In the top left panel the time spectrum in gray is integrated over all detected energies, while the spectrum in white is gated on 1332-keV energy detected in SeGA.

detector [3,7]. A set of average pulses (called “superpulses”) was constructed from the coincidence data as follows. For each segment of a SeGA detector, a subset of events corresponding to the full absorption of the 1332-keV  $\gamma$  ray in this segment was selected under a condition that the  $\gamma$  ray was detected in the time peak corresponding to the prompt coincidence with the CsF detector as seen in Fig. 8. The waveforms for all events in this subset were aligned to minimize deviations between the reference signals and then averaged. The size of a data set for a superpulse measurement varied between  $\sim 100$  and  $\sim 500$  events depending on the location of a detector and the segment.

Substantial differences between waveforms for superpulses and for corresponding individual events were observed and are believed to indicate sensitivity of SeGA detectors to  $\gamma$ -ray position identification with sub-segment resolution. An example comparison of two sets of waveforms with a superpulse for segment E2 of one of the SeGA detectors is illustrated by Fig. 9. Significant variations of the risetimes for the core and the hit-segment signals are observed; the same is true for amplitudes and shapes of signals induced on segments other than E2. The implementation of the signal decomposition algorithm and identification of  $\gamma$ -ray interaction points based on measured waveforms is an ongoing research project and will be reported in subsequent papers. For the purpose of the work presented here, Fig. 9 and other presented results clearly demonstrate the ability of DDAS to provide data needed for  $\gamma$ -ray tracking in NSCL’s in-beam experiments with SeGA detectors.

#### 7.6. S800/SeGA event building

The integration of DDAS SeGA with other detection systems at NSCL discussed in Section 6 was tested in several experiments; a result of a test with a stable beam of  $^{24}\text{Mg}$  at 61 MeV/u is

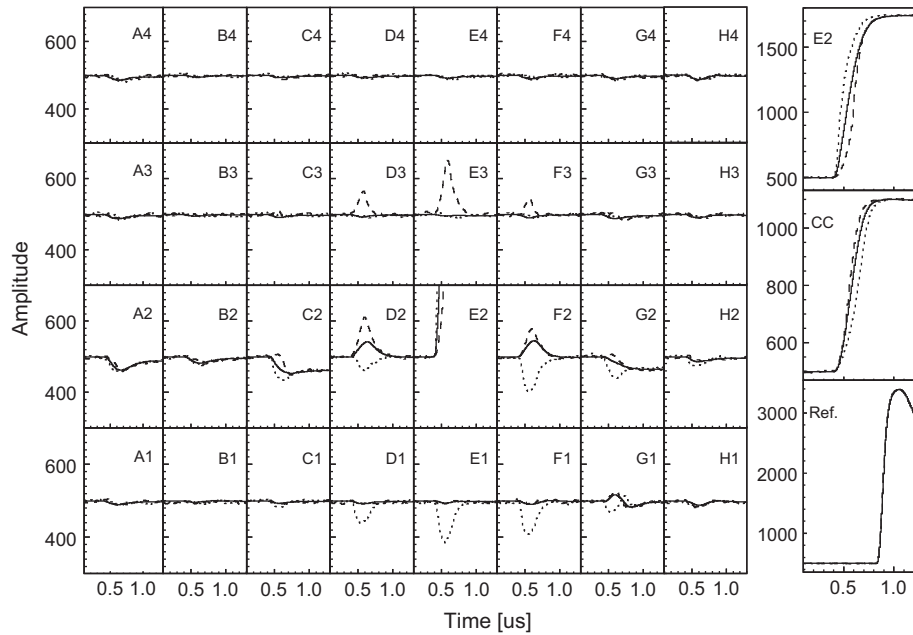


**Fig. 9.** Comparison of the set of waveforms for a superpulse (solid) and two individual events (dashed and dotted) for full absorption of the 1332-keV  $\gamma$ -ray energy in segment E2 of a SeGA detector. The waveforms for all three sets were aligned to minimize deviations between the reference signals shown in the lower right panel; the reference was provided by a coincident 1173-keV  $\gamma$ -ray detected in a CsF fast scintillator.

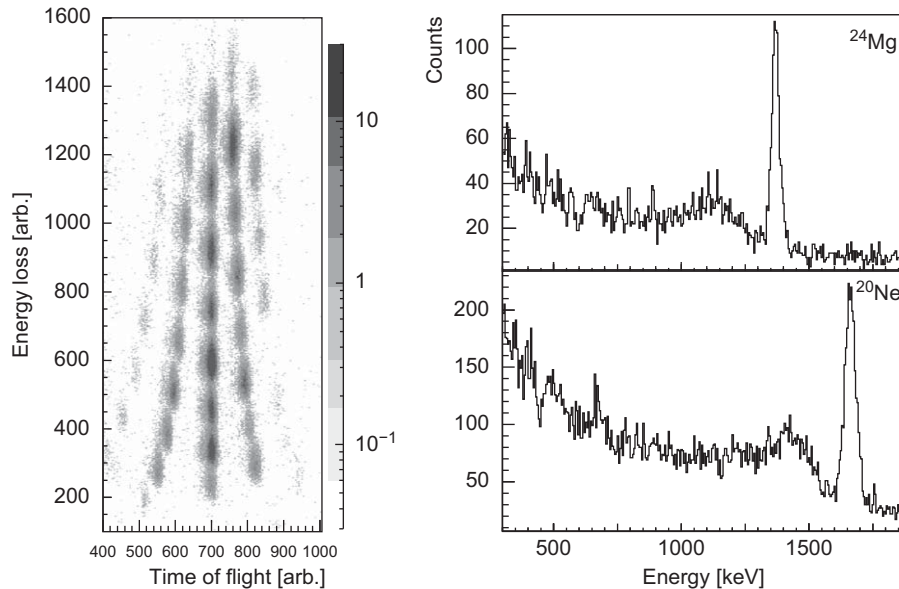


**Fig. 10.** Results of an in-beam test from a DDAS SeGA S800 experiment performed with a stable beam of  $^{24}\text{Mg}$  at the energy of 61 MeV/u. (Left) Particle identification plot of the time-of-flight from the target to the focal plane of the S800 spectrograph vs. the energy loss in the S800 ionization chamber, see Ref. [2] for further details. Note the line of  $N = Z$  nuclei at the time-of-flight of  $\sim 700$  units. (Right) Particle gated  $\gamma$ -ray spectra for (top) inelastically scattered  $^{24}\text{Mg}$  nuclei and (bottom)  $^{20}\text{Ne}$  nuclei produced in the projectile fragmentation.

illustrated in Fig. 10. In this experiment, several  $N \sim Z$  nuclei were populated by projectile fragmentation of the primary beam on a 1 mm thick Be target at the target position of the S800 spectrograph. The mass and charge of the reaction products were extracted on an event-by-event basis from the time-of-flight and energy loss information. The time-of-flight was measured between a plastic scintillator in the object of the S800 and the E1 plastic scintillator in the S800 focal plane. The energy loss measurement was performed by the ionization chamber at the S800 focal plane [8]. The resulting particle identification plot is shown in the left panel of Fig. 10. The right panel of the same figure shows Doppler-corrected spectra reconstructed from the DDAS data stream for inelastically scattered primary beam of

$^{24}\text{Mg}$  and for  $^{20}\text{Ne}$  produced in primary projectile fragmentation. The Doppler correction algorithm used in this analysis is the same as used in experiments with the analog SeGA data acquisition system [1] and yields a comparable 2% FWHM energy resolution.

## 8. Conclusions

The DDAS system has been deployed for several source and in-beam experiments at NSCL and has performed up to specifications. Current efforts are concentrated on the implementation of  $\gamma$ -ray tracking in SeGA detectors enabled by the application of the digital signal processing from the DDAS data. The combination of

$\gamma$ -ray tracking and tracking of heavy ions in the S800 offers an opportunity to significantly improve  $\gamma$ -ray energy resolution in measurements at NSCL through more accurate Doppler corrections. This will have a direct impact on the sensitivity of Doppler-shift based lifetime measurements [9]. For example, in the Recoil Distance Method (RDM) the sensitivity to lifetime effects depends on the magnitude of the Doppler-shift as compared to Doppler broadening, which defines energy resolution. Reduced Doppler-broadening allows for thinner degraders to be used in RDM measurements; as a result access to shorter lifetimes is possible. Moreover, measurements with multiple degraders can be envisioned, allowing for a lifetime to be extracted without a need to change the target-degrader distance. Also, better energy resolution opens an opportunity for efficient coincidence measurements which can eliminate feeding corrections present in knock-out and fragmentation schemes. All of the above will play a significant role in pushing the precision lifetime measurements towards the neutron drip-line. Several data sets for RDM experiments with DDAS SeGA S800 have been obtained and are currently under analysis.

### Acknowledgments

The DDAS project was funded by the US National Science Foundation (NSF) Grant Major Research Instrumentation Program

Grant no. 0420778. This work is supported in parts by the NSF Grant no. PHY-0606007. HC acknowledges support from the National Science and Engineering Research Council (NSERC) of Canada. The authors would like to acknowledge the support of the NSCL Computer Group in completing the projects.

### References

- [1] W.F. Mueller, J.A. Church, T. Glasmacher, D. Gutknecht, G. Hackman, P.G. Hansen, Z. Hu, K.L. Miller, P. Quinn, Nucl. Instr. and Meth. A 466 (2001) 492.
- [2] D. Bazin, J.A. Caggiano, B.M. Sherrill, J. Yurkon, A. Zeller, Nucl. Instr. and Meth. B 204 (2003) 629.
- [3] I.Y. Lee, Nucl. Instr. Meth. A 422 (1999) 195.
- [4] H. Tan, W. Hennig, M. Walby, A. Fallu-Labruyere, J. Harris, D. Breus, P. Grudberg, W.K. Warburton, C. Vaman, T. Glasmacher, P. Mantica, D. Miller, K. Starosta, P. Voss, in: Nuclear Science Symposium Conference Record, NSS '08, IEEE, 2008, p. 3196.
- [5] W. Hennig, H. Tan, M. Walby, P. Grudberg, A. Fallu-Labruyere, W.K. Warburton, C. Vaman, K. Starosta, D. Miller, Nucl. Instr. and Meth. B 261 (2007) 1000.
- [6] B. Bruyneel, P. Reiter, A. Wiens, J. Eberth, H. Hess, G. Pascovici, N. Warr, D. Weisshaar, Nucl. Instr. and Meth. A 599 (2009) 196.
- [7] M. Descovich, I.Y. Lee, P. Fallon, M. Cromaz, A.O. Macchiavelli, D.C. Radford, K. Vetter, R.M. Clark, M.A. Deleplanque, F.S. Stephens, D. Ward, Nucl. Instr. and Meth. A 553 (2005) 535.
- [8] J. Yurkon, D. Bazin, W. Benenson, D.J. Morrissey, B.M. Sherrill, D. Swan, R. Swanson, Nucl. Instr. and Meth. A 422 (1999) 291.
- [9] K. Starosta, P. Adrich, A. Dewald, D. Miller, V. Moeller, C. Vaman, P. Voss, Acta Phys. Pol. B 40 (2009) 789.